RESEARCH ARTICLE

Aligned fibers enhance nerve guide conduits when bridging peripheral nerve defects focused on early repair stage

Qi Quan[1, #], Hao-Ye Meng[1, 3, #], Biao Chang[2, #], Guang-Bo Liu[1], Xiao-Qing Cheng[1], He Tang[1], Yu Wang[1, 4], Jiang Peng[1, 4], Qing Zhao[4, 5, *], Shi-Bi Lu[1, *]

1 Department of Orthopedic Surgery, Key Laboratory of Musculoskeletal Trauma & War Injuries PLA, Beijing Key Lab of Regenerative Medicine in Orthopedics, Chinese PLA General Hospital, Beijing, China
2 Department of Laser Medicine, Chinese PLA General Hospital, Beijing, China
3 School of Materials Science and Engineering, University of Science & Technology Beijing, Beijing, China
4 Neural Regeneration Co-innovation Center of Jiangsu Province, Nantong, Jiangsu Province, China
5 Department of Orthopedic Surgery, First Affiliated Hospital of PLA General Hospital, Beijing, China

Funding: *This study was supported by the National Natural Science Foundation of China, No. 31771052 (to YW); the National Basic Research Program of China (973 Program), No. 2014CB542201 (to JP); the National Key Research and Development Program of China, No. 2016YFC1101601 (to QZ), 2017YFA0104702 (to YW); the PLA General Hospital Translational Medicine Project of China, No. 2016TM-030 (to QZ); the Beijing Municipal Natural Science Foundation of China, No. 7172202 (to YW); the PLA Youth Training Project for Medical Science, China, No. 16QNP144 (to YW); the Beijing Municipal Science and Technology Project, China, No. Z161100005016059 (to YW).*

Graphical Abstract

A nerve guide conduit (NGC) with a channel fabricated by highly aligned nanofibers not only exhibited sufficient mechanical strength and micro bionic structure, but was useful for the regeneration of Schwann cells and axons

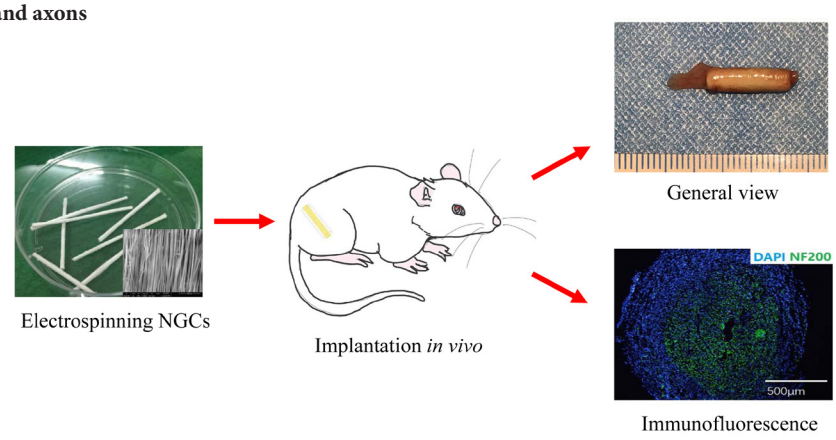

Correspondence to:
Shi-Bi Lu, PhD, MD, lusb301@126.com;
Qing Zhao, PhD, MD, zqmd301@126.com.

#These authors contributed equally to this work.

orcid:
0000-0003-1493-4042 (Qi Quan)
0000-0001-9055-6755 (Qing Zhao)

doi: *10.4103/1673-5374.249239*

Received: *April 18, 2018*
Accepted: *August 23, 2018*

Abstract

Nerve conduits enhance nerve regeneration in the repair of long-distance peripheral nerve defects. To help optimize the effectiveness of nerve conduits for nerve repair, we developed a multi-step electrospinning process for constructing nerve guide conduits with aligned nanofibers. The alignment of the nerve guide conduits was characterized by scanning electron microscopy and fast Fourier transform. The mechanical performance of the nerve guide conduits was assessed by testing for tensile strength and compression resistance. The biological performance of the aligned fibers was examined using Schwann cells, PC12 cells and dorsal root ganglia *in vitro*. Immunohistochemistry was performed for the Schwann cell marker S100 and for the neurofilament protein NF200 in PC12 cells and dorsal root ganglia. In the *in vivo* experiment, a 1.5-cm defect model of the right sciatic nerve in adult female Sprague-Dawley rats was produced and bridged with an aligned nerve guide conduit. Hematoxylin-eosin staining and immunohistochemistry were used to observe the expression of ATF3 and cleaved caspase-3 in the regenerating matrix. The recovery of motor function was evaluated using the static sciatic nerve index. The number of myelinated fibers, axon diameter, fiber diameter, and myelin thickness in the distal nerve were observed by electron microscopy. Gastrocnemius muscle mass ratio was also determined. The analyses revealed that aligned nanofiber nerve guide conduits have good mechanical properties and can induce Schwann cells, PC12 cells and dorsal root ganglia to aggregate along the length of the nanofibers, and promote the growth of longer axons in the latter two (neuronal) cell types. The aligned fiber nerve conduits increased the expression of ATF3 and cleaved caspase-3 at the middle of the regenerative matrix and at the distal nerve segment, improved sciatic nerve function, increased muscle mass of the gastrocnemius muscle, and enhanced recovery of distal nerve ultrastructure. Collectively, the results show that highly aligned nanofibers improve the performance of the nerve conduit bridge, and enhance its effectiveness in repairing peripheral nerve defects.

Key Words: *nerve regeneration; nerve guide conduit; electrospinning; peripheral nerve injury; aligned fiber; sciatic nerve; structure; mechanical function; nerve scaffold; nanofiber; neural regeneration*

Chinese Library Classification No. *R458; R318.08; R741*

Introduction

Peripheral nerve injury is becoming increasingly common with the rise in the number of traumatic injuries, terrorist attacks, natural disasters, and traffic accidents. Peripheral nerves have a greater capacity to regenerate than the central nervous system (Coleman and Freeman, 2010; Gu et al., 2014; Wang et al., 2014). However, this capacity is limited by the degree of damage (Chang et al., 2016). Complete peripheral nerve transection is the most severe form of damage, particularly when there is a large defect or "gap" (Deumens et al., 2010). Although autologous grafts (autografts) are considered the best therapy, the optimal treatment for large nerve defects remains unclear (Ray and Mackinnon, 2010; Haastert-Talini et al., 2013; Quan et al., 2016). Autografts have several drawbacks, including sensory deficits caused by surgery to the donor nerve, scars, limited nerve sources, formation of traumatic neuromas, difficulties repairing long segments or special parts of the peripheral nerve defect, and the possibility that the nerve fibers will not match (Bertleff et al., 2005; Quan et al., 2016). Therefore, nerve scaffolds produced by tissue engineering might be an alternative to conventional transplantation (Bellamkonda, 2006; de Luca et al., 2014).

It is generally recognized that peripheral nerve regeneration is mainly determined by axonal outgrowth (Schnell et al., 2007; Ray and Mackinnon, 2010; Meyer et al., 2016). Clinically, for small segmental nerve defects, end-to-end or end-to-side suture is usually performed (Battiston et al., 2007; Geuna et al., 2017). For large segmental nerve defects, nerve allografts, autologous and alloplastic nerve conduits are usually employed to provide a bridge for axonal outgrowth (Geuna et al., 2007; Tos et al., 2007). Some studies have shown that aligned nanofibers can stimulate and promote Schwann cell orientation and axon growth *in vitro* (Chew et al., 2007; Ayres et al., 2008; Chew et al., 2008; Zhu et al., 2011). Accordingly, we hypothesized that placing aligned nanofibers within a nerve guide conduit may be a promising strategy to accelerate nerve regeneration (Johansson and Dahlin, 2014). This design may provide a biomimetic microenvironment for peripheral nerve regeneration. We developed a multi-step electrospinning process to mimic the perineurium within a nerve scaffold constructed by tissue engineering for peripheral nerve regeneration. There are two primary goals of this study: (1) To generate a nerve guide conduit with a channel fabricated by highly aligned nanofibers and to test its mechanical properties; (2) To perform *in vitro* cytological assays and *in vivo* experiments to assess peripheral nerve regeneration using this nerve guide conduit.

Materials and Methods

Study design includes *in vitro* and *in vivo* studies. **Figure 1** shows our experimental design. This study was approved by the Ethics Committee of the Chinese PLA General Hospital, Beijing, China (approval number: 2016-x9-07) in September, 2016.

Construction of the aligned polycaprolactone nanofiber membrane with 2% chitosan

An aligned membrane composed of polycaprolactone (Sigma-Aldrich, St. Louis, MO, USA) and 2% chitosan was dissolved in hexafluoro-2-propanol (Sigma-Aldrich) and stirred for approximately 12 hours at 25°C to obtain an 8% (w/v) solution. The solution was electrospun from a 2.5 mL syringe attached to a needle with a diameter of 0.4 mm. The volumetric flow rate was set at 1.5 mL/h. High voltage (15 kV) was applied to the needle when the fluid jet was ejected, and low voltage (−7.5 kV) was applied to the collector. The plane needle tip was required to generate a well-defined Taylor cone. Before the coverslips were fixed on the aluminum collector roller, an 8% (w/v) solution of 85:15 poly(lactic-co-glycolic acid) (Sigma-Aldrich) was used to coat the coverslips. The poly(lactic-co-glycolic acid) was dried to a thin film (30–45 minutes). Coverslips (15 × 15 mm^2) were fixed to a grounded aluminum collector roller. A target rotating at approximately 2800 r/min was used to generate the fibers.

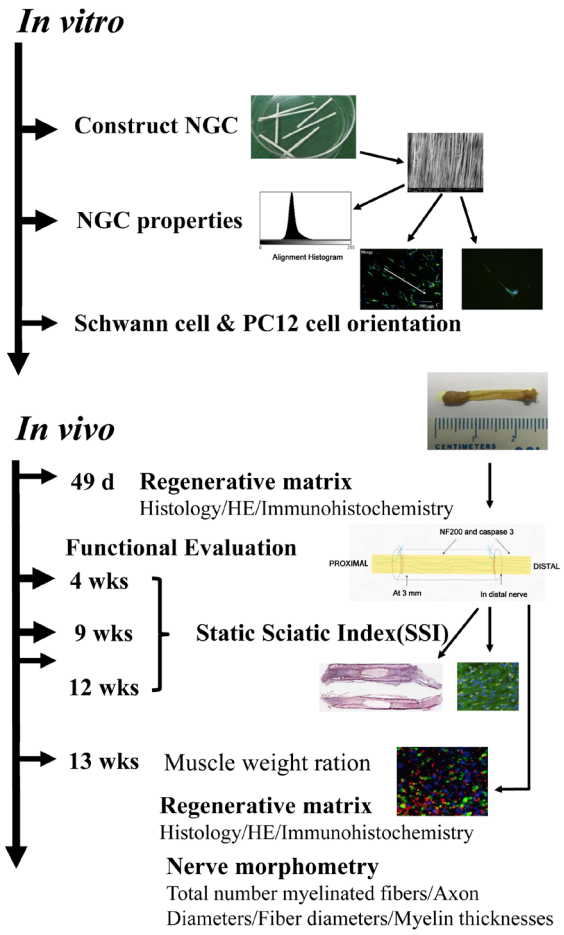

Figure 1 Illustration of the various steps of the comprehensive *in vitro* and *in vivo* analyses.
NGC: Nerve guide conduit; HE: hematoxylin-eosin; d: days; wks: weeks.

Construction of nerve guide conduits with highly aligned nanofibers

After deposition of the longitudinally aligned fibers of the roller, a micro-pipe was placed on the aligned membrane along its long axis, unrolled, and deposited in a randomly oriented layer. The experimental conditions were as de-

scribed above. After electrospinning was completed, the nerve guide conduits were placed at room temperature for 24 hours to remove residual hexafluoro-2-propanol, and then cut into lengths of approximately 1.5 cm, and the micro-pipe was removed. The nerve guide conduits were sterilized before *in vitro* and *in vivo* analyses.

Structural evaluation of the aligned nanofiber membrane and nerve guide conduits

The nerve scaffold and conduits were sputter-coated with gold, and images were captured on a scanning electron microscope (Carl Zeiss, Oberkochen, Germany). To analyze fiber alignment, the images of the nanofiber membrane and nerve guide conduit were converted into an appropriate format for MATLAB software (R2015b, MATLAB Inc., Natick, MA, USA) and transformed using the two-dimensional fast Fourier transform function (Zhu et al., 2011).

Mechanical testing

The compressive and tensile strength of nerve guide conduits were tested using a mechanical testing machine (BOSS 5100, Flemingham, MA, USA), with 10, 50 and 100 repeats of cyclic compression and a radial compressive stiffness at 50% strain of the aligned and random nerve guide conduits.

Nerve cell culture

Schwann cells were isolated and purified from Sprague-Dawley rats using a previously established protocol (Forciniti et al., 2014). In short, sciatic nerves and the brachial plexus were excised from 10 specific-pathogen-free 2-day-old Sprague-Dawley rats (Vital River Laboratory Animal Technology Co., Ltd., Beijing, China; license number SCXK (Jing) 2015-0001) and enzymatically dissociated in 1% collagenase and 0.125% trypsin. Schwann cells were cultured in Dulbecco's modified Eagle medium/F12 supplemented with 10% fetal bovine serum, 10 ng/mL heregulin-β1 (Sigma-Aldrich) and 2 mM forskolin (Sigma-Aldrich) in a 25 cm^2 cell culture flask in an atmosphere containing 5% CO_2 at 37°C. The culture medium was replaced every 3 days. Aligned nanofibrous scaffolds on 15-mm coverslips were placed in six-well plates. Samples were washed three times with phosphate-buffered saline and immersed in culture medium overnight before seeding. Cells were seeded on scaffolds at a density of 90–110 cells/well in a six-well plate (9.6 cm^2) and incubated for 5 days until fixation with 4% paraformaldehyde.

PC12 cells from American Type Culture Collection (Rockville, MD, USA) were plated at approximately 20–30 cells/mm^2 and incubated for 3 days without medium change.

For dorsal root ganglion culture, the spinal cords from three 2-day-old Sprague-Dawley rats were dissected out, and the dorsal root ganglions were carefully removed. The dorsal root ganglion was allowed to adhere to the aligned polycaprolactone nanofiber membrane for approximately 3–5 hours before the culture medium was added, which we consider critical for successful culture. The dorsal root ganglion was incubated for approximately 4 days without medium change. The experiments were approved by the Ethics Committee of the Chinese PLA General Hospital, Beijing, China (approval number: 2016-x9-07) in September, 2016.

Immunohistochemistry

To detect Schwann cells, samples were incubated at 4°C with rabbit anti-mouse S100 antibody (Abcam, Cambridge, UK) diluted 1:600 in 0.5% Triton-X 100 and 0.5% bovine serum albumin in phosphate-buffered saline overnight. The following day, samples were washed with phosphate-buffered saline, incubated with Alexa Fluor-488 conjugated goat anti-rabbit IgG (Abcam) diluted 1:200 in phosphate-buffered saline for 1 hour at room temperature, and washed 3 × 5 minutes with phosphate-buffered saline. Finally, samples were mounted with 4,6-diamino-2-phenylindole and coverslipped.

For PC12 cells and dorsal root ganglions, we analyzed neurofilament protein. Samples were washed in phosphate-buffered saline following treatment with 4% warm paraformaldehyde and incubated at 4°C with mouse anti-neurofilament 200 (NF200) antibody (Abcam) diluted 1:200 in 0.5% Triton-X 100 and 0.5% bovine serum albumin in phosphate-buffered saline overnight. The following day, samples were washed with phosphate-buffered saline, incubated with Alexa Fluor-488-conjugated goat anti-mouse IgG (Invitrogen Molecular Probes, Carlsbad, CA, USA) diluted 1:200 in phosphate-buffered saline for 1 hour at room temperature, and washed 3 × 5 minutes with phosphate-buffered saline. Finally, samples were mounted with 4,6-diamino-2-phenylindole and coverslipped. A fluorescence microscope (BX51; Olympus, Tokyo, Japan) was used to observe the cells.

***In vivo* implantation**

A total of 60 adult specific-pathogen-free female Sprague-Dawley rats, 12 weeks of age and weighing 220 ± 15 g (Vital River Laboratory Animal Technology Co., Ltd., Beijing, China), were used. The aligned scaffold group contained 24 rats, the random scaffold group contained 24 rats, and the autograft group contained 12 rats. The rats were anesthetized by intraperitoneal injection of 2% sodium pentobarbital solution (30 mg/kg body weight; Sigma-Aldrich) prior to surgery. The rats were placed in the prone position, and the right hind limb was disinfected. A 2-cm incision was made, and the sciatic nerve was isolated. Using a surgical microscope (C2.3, Heine, Herrsching, Germany), an approximately 1-cm segment of the sciatic nerve was removed, leaving a gap that was bridged by the nerve guide conduit. Both nerve ends were sutured in place with two 8–0 nylon monofilament sutures. The wound was closed with 4–0 nylon sutures.

Analyses of regenerative matrix within the tubes

After 49 days, the nerve guide conduits were removed (the conduit and 2 mm of the proximal and 2 mm of the distal nerve segment), placed in Stefanini fixative (Solarbio, Beijing, China) at 4°C for 24 hours, and incubated in 20% sucrose solution overnight for cryoprotection. The tissues were frozen and longitudinally sectioned into 7-μm-thick slices and collected on glass slides.

For neurofilaments, the samples without nerve guide

conduits were washed in phosphate-buffered saline and incubated at 4°C with mouse anti-NF200 antibody (Abcam) diluted 1:800 in 0.5% Triton-X 100 and 0.5% bovine serum albumin in phosphate-buffered saline overnight. The following day, samples were washed with phosphate-buffered saline, incubated with Alexa Fluor-488-conjugated goat anti-mouse IgG diluted 1:200 in phosphate-buffered saline for 1 hour at room temperature, and washed 3 × 5 minutes with phosphate-buffered saline. Finally, samples were mounted with 4,6-diamino-2-phenylindole and coverslipped.

Activating transcription factor 3 (ATF3) and cleaved caspase-3 were used to detect activated and apoptotic Schwann cells, respectively. The samples without nerve guide conduits were washed in phosphate-buffered saline and incubated at 4°C with mouse anti-ATF3 antibody (Abcam) or cleaved caspase-3 rabbit anti-mouse (Abcam) antibody diluted 1:200 in 0.5% Triton-X 100 and 0.5% bovine serum albumin in phosphate-buffered saline overnight. The following day, samples were washed with phosphate-buffered saline, incubated with Alexa Fluor-488 or -594-conjugated goat anti-mouse IgG (Abcam) diluted 1:200 in phosphate-buffered saline for 1 hour at room temperature, and washed 3 × 5 minutes with phosphate-buffered saline. Finally, samples were mounted with 4′,6-diamino-2-phenylindole and coverslipped.

For qualitative analyses, representative photomicrographs of hematoxylin-eosin-stained and antibody-labeled sections were taken on a fluorescence microscope and analyzed with ImageJ software (National Institutes of Health, Bethesda, MD, USA). Briefly, the number of axons (NF200 staining) was assessed in the distal nerves. The numbers of ATF3- and cleaved caspase-3-positive cells in each section (20× magnification) in the matrix were determined. The total number of 4′,6-diamino-2-phenylindole-stained cells was also counted.

Functional evaluation

Over the long-term observation period of 3 months (3, 9 and 12 weeks) following nerve reconstruction, functional motor recovery was assessed with the CATWalk gait analysis system (Noldus, Wageningen, Netherlands). Static sciatic index was calculated as described previously (Haastert-Talini et al., 2013).

Nerve morphometric analysis

The distal nerve segment samples were combined for nerve histology after 12 weeks. Tissues were subjected to an initial fixation with glutaraldehyde-containing fixatives and post-fixed in 1% osmium tetroxide. After dehydration, 2.5-μm transverse sections were cut and stained with toluidine blue. The total number of myelinated fibers, axon diameter, fiber diameter and myelin thickness in the different groups were examined under the transmission electron microscope (Hitachi, Tokyo, Japan).

Muscle weight ratio analysis

The rats were sacrificed after 12 weeks, and the gastrocnemius muscles of both lower limbs were excised and weighed to determine the muscle weight ratio (ipsilateral [g]/contralateral [g]).

Histomorphometric assessment of regenerated nerve tissue

After the functional tests were performed, the rats were sacrificed and the regenerated tissues were harvested for histomorphometric assessment. The samples were fixed in Stefanini solution at 4°C for 24 hours. Serial 7-μm sections were washed in phosphate-buffered saline and incubated at 4°C with mouse anti-NF200 antibody (Abcam) or goat anti-mouse choline acetyltransferase (ChAT) antibody (Abcam) diluted 1:200 or 1:50, respectively, in 0.5% Triton-X 100 and 0.5% bovine serum albumin in phosphate-buffered saline overnight. The following day, samples were washed with phosphate-buffered saline, incubated with Alexa Fluor-488 or -555 conjugated goat anti-mouse IgG (Abcam) diluted 1:200 in phosphate-buffered saline for 1 hour at room temperature, and washed 3 × 5 minutes with phosphate-buffered saline. Finally, samples were mounted with 4,6-diamino-2-phenylindole and coverslipped. A fluorescence microscope was used to observe the samples at 20× magnification. ImageJ software was used for qualitative analyses.

Statistical analysis

All data are expressed as the mean ± SEM. SPSS Statistics ver. 22.0 (IBM Corp., Armonk, NY, USA) was used for data analyses. The *P*-values were based on Fisher's exact method for 2 × 2 cross tabulation or on one-way analysis of variance. *P*-values < 0.05 were considered statistically significant.

Results

Characterization of nanofiber nerve guide conduits

Electrospun nanofibrous nerve guide conduits were produced with a diameter of 1.5 mm. The aligned poly(lactic-co-glycolic acid) nanofiber internal surface of the nerve guide conduit is shown in **Figure 2**. The fast Fourier transform technique was used to analyze fiber alignment (**Figure 2B**).

Mechanical properties of nanofiber nerve guide conduits

The tensile load on aligned nanofiber nerve guide conduits at approximately 50% tensile strain appears to show a turning point (**Figure 3A**). This could be a result of breakage of the aligned fibers on the luminal surface. As shown in **Figure 3B**, the compression performances of aligned nanofiber nerve guide conduits were better than those of random nanofiber nerve guide conduits. A cyclic compression test was performed to assess the mechanical properties of the aligned and random nanofiber nerve guide conduits. The nanofiber nerve guide conduits had good compression recovery ability, even after being compressed 100 times (**Figure 3C**).

Schwann cell morphology on the scaffolds

Schwann cells were seeded on aligned or random scaffolds for 5 days. Schwann cells were oriented along the direction of the aligned nanofibers and clustered around the fibers in a longitudinal manner (**Figure 4**).

Morphology of PC12 cells and dorsal root ganglions on the scaffolds

Similar results were obtained with PC12 cells and dorsal

root ganglions. The PC12 cells and dorsal root ganglions in the aligned nanofiber nerve guide conduits exhibited longer axons compared with those seeded on random fibers (**Figures 5** and **6**).

Nerve regeneration in aligned nanofiber nerve guide conduits

No bridging matrix was formed at 21 or 35 days. We selected the regenerative matrix that formed at 49 days for further analyses (**Figure 7**). Given that several studies have indicated that it is difficult to accurately measure the length of axonal outgrowth, the presence of axons was used to assess axonal outgrowth (Meyer et al., 2016; Stenberg et al., 2016). Axons were observed in the middle of the formed matrices in 6/7 (85%) of the random nanofiber nerve guide conduits and in 7/7 (100%) of the aligned nanofiber nerve guide conduits. In the distal nerve segment, neurofilament-positive staining was detected in 4/7 (57%) of the random nanofiber nerve guide conduits and in 7/7 (100%) of the aligned nanofiber nerve guide conduits. Chi-square tests showed a statistically significant difference in the presence of new neurofilaments in the distal nerve segment between the aligned and random nanofiber nerve guide conduits; however, there were no differences in the middle segment. In addition, there were no differences in the number of foot ulcers (**Table 1** and **Figure 7**).

Table 1 Axons and foot ulcers in the aligned and random nanofiber NGC groups

Item	Aligned scaffold group	Random scaffold group	*P*-values
Presence of axons (NF200 staining; animals with ulcer/group number)			
In nerve guide	7/7	6/7	0.299
In distal nerve	7/7	4/7	0.035
Presence of foot ulcer (animals with ulcer/group number)	0/7	3/7	0.096

P-values are based on Fisher's method on 2 × 2 cross tabulation (Fisher's exact test). NGC: Nerve guide conduit; NF200: neurofilament.

The percentages of activated (ATF3-positive) and apoptotic (cleaved caspase-3-positive) Schwann cells were evaluated at three locations: at 3 mm in the regenerative matrix, the middle of the regenerative matrix, and the distal nerve segment. There were no differences in ATF3 or cleaved caspase-3 staining between the aligned and random nanofiber nerve guide conduits at 3 mm into the regenerative matrix ($P = 0.083$ for ATF3; $P = 0.38$ for cleaved caspase-3). There were significant differences between the aligned and random nerve guide conduits at the middle of the regenerative matrix and at the distal nerve segment. ATF3-positive cells appeared more numerous in the aligned scaffold group than in the random scaffold group both in the nerve conduit and in the distal nerve. A similar result was obtained for caspase-3-positive cells in the nerve conduit. However, in the distal nerve segment, caspase-3-positve cells were more numerous in the random scaffold group than in the aligned scaffold group. The number of 4′,6-diamino-2-phenylindole-stained cells at 3 mm into the regenerated matrix did not differ between the groups. However, there was a significant difference in the middle of the nerve guide segment (**Table 2**).

Table 2 Regenerative matrix in rats evaluated 49 days after implantation

	Aligned scaffold group	Random scaffold group	*P*-values
ATF3 stained cells (% of total)			
At 3 mm of the regenerative matrix	1.31	1.10	0.083
In nerve guide	1.07	0.59	0.001
In distal nerve	4.32	2.85	0.001
Cleaved caspase-3 stained cells (% of total)			
At 3 mm of the regenerative matrix	1.82	1.41	0.38
In nerve guide	1.39	0.93	0.031
In distal nerve	6.07	7.34	0.015
Total number of DAPI stained cells (n/mm^2)			
At 3 mm of the regenerative matrix	1007	951	0.092
In nerve guide	901	762	0.012
In distal nerve	1260	1234	0.781

P-values are based on Fisher's method on 2 × 2 cross tabulation (Fisher's exact test). ATF3: Activating transcription factor 3.

Long-term observation of sciatic nerve regeneration in rats implanted with aligned or random nanofiber nerve guide conduits

Sciatic nerve functional recovery in Sprague-Dawley rats was evaluated using muscle weight ratios and the static sciatic index. Although there was a trend towards faster sciatic nerve functional recovery in the aligned scaffold group than in the random scaffold group, the differences were not statistically significant (**Figure 8A**).

After the final noninvasive measurements were obtained, the muscle weight ratios of the gastrocnemius muscle were determined. No differences were observed among the experimental groups (**Figure 8B**). Regenerated tissue was removed from the nanofiber nerve guide conduits after 120 days for immunofluorescence analysis (**Figure 9**).

The nerve tissue was immunostained for NF200 and ChAT to demonstrate nerve fibers within the regenerated nerve cables (**Figure 10**). The total number of myelinated fibers, axon diameters, fiber diameters and myelin thicknesses in the different groups are shown in **Figure 11**. The total number of myelinated fibers was significantly different between the healthy nerve ($n = 8$) and surgery groups (aligned scaffold group: $n = 8$; random scaffold group: $n = 8$), but there were no differences between the aligned and random scaffold groups. Similar results were obtained for axon and fiber diameters and myelin thickness.

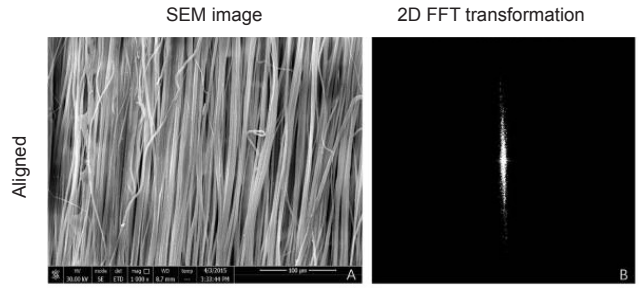

Figure 2 Scanning electron microscope (SEM) and fast Fourier transform of the aligned fiber nerve guide conduit.
(A) Alignment analysis of fibers on the luminal surface of the nerve guide conduit (scanning electron microscope). Scale bar: 100 μm. (B) Two-dimensional fast Fourier transform (FFT) image in black and white.

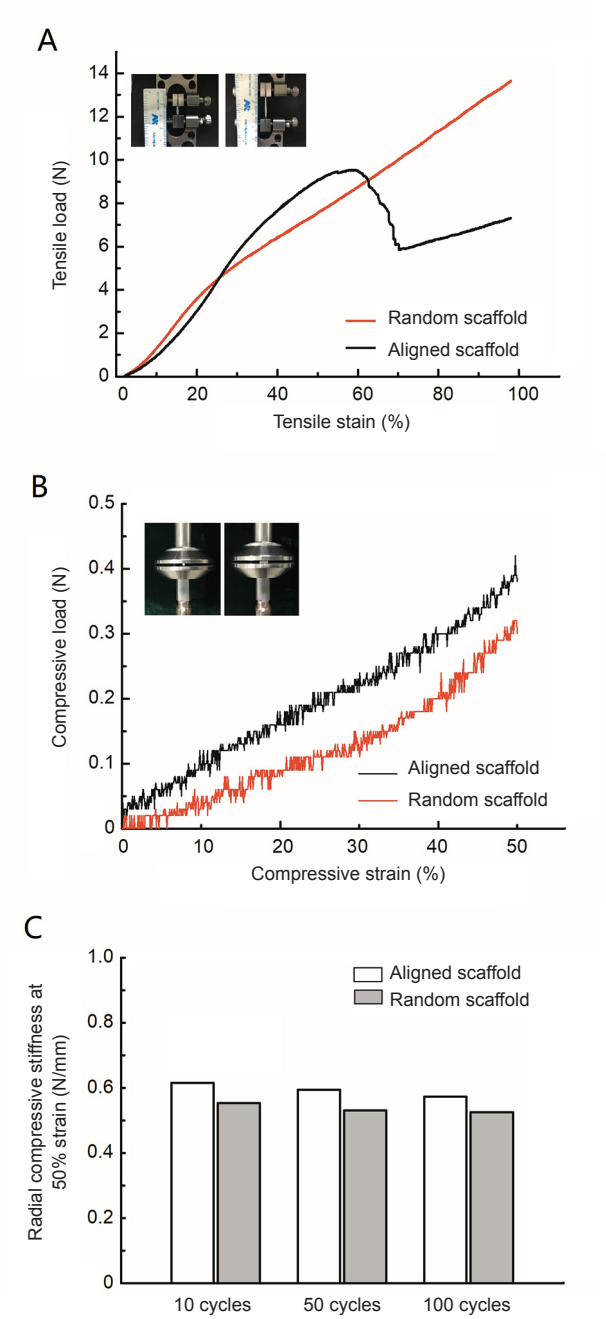

Figure 3 Mechanical analysis of the nanofiber NGC.
(A) Curves of tensile strain and tensile load. (B) Curves of compressive strain and compressive load. (C) Radial compressive stiffness at 50% strain of the NGC at different cycles. Because the conduit was resilient, we only made one measurement after compression, and therefore, there is no error value. NGC: Nerve guide conduit.

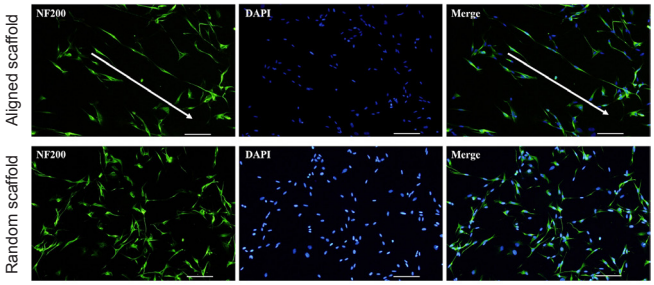

Figure 4 Morphology of Schwann cells on the aligned scaffold (immunohistochemistry).
Schwann cells in the aligned fiber scaffold appear aligned (arrows). Schwann cells oriented along the direction of the aligned nanofibers and clustered around the fibers in a longitudinal manner. The fluorescent indicator for NF200 is Alexa Fluor-488 (green). Scale bars: 100 μm. NF200: Neurofilament 200; DAPI: 4′,6-diamidino-2-phenylindole.

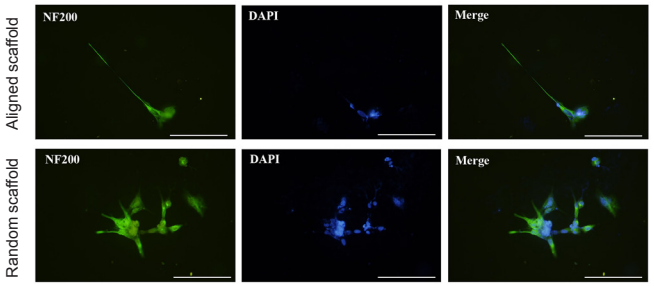

Figure 5 Morphology of PC12 cells on the aligned scaffold (immunohistochemistry).
PC12 cells in the aligned nanofiber nerve guide conduit exhibited longer axons compared with those seeded on random fibers. The fluorescent indicator for S-100 is Alexa Fluor-488 (green). Scale bars: 20 μm. NF200: Neurofilament 200; DAPI: 4′,6-diamidino-2-phenylindole.

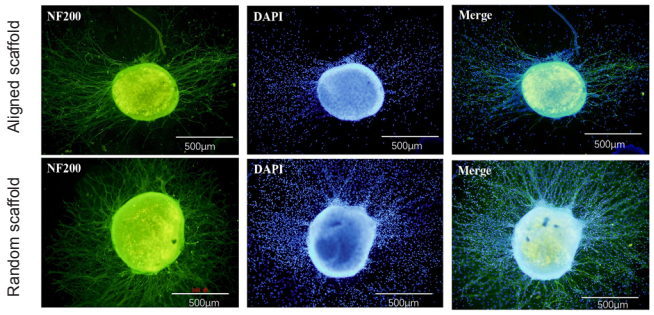

Figure 6 Morphology of a dorsal root ganglion on the scaffold (immunohistochemistry).
The dorsal root ganglion in the aligned nanofiber nerve guide conduit exhibited longer axons compared with that seeded on random fibers. The fluorescent indicator for S-100 is Alexa Fluor-488 (green). Scale bars: 500 μm. NF200: Neurofilament 200; DAPI: 4′,6-diamidino-2-phenylindole.

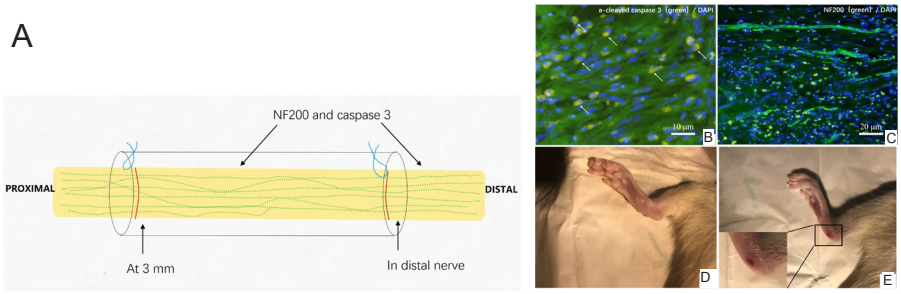

Figure 7 Regenerative tissue in the rat sciatic nerve defect bridged with the aligned fiber nerve guide conduit.
(A) Analysis of regenerative matrix 49 days after implantation. (B) Tissue at 3 mm within the matrix in sections stained with cleaved caspase-3 antibody (green, Alexa Fluor 488, apoptotic cells). (C) NF200 antibody (green, Alexa Fluor 488, axons). Scale bars: 10 μm in B, 20 μm in C. (D, E) Comparison of the feet in rats implanted with aligned (D) and random (E) nanofiber nerve guide conduits. NF200: neurofilament 200; DAPI: 4′,6-diamidino-2-phenylindole.

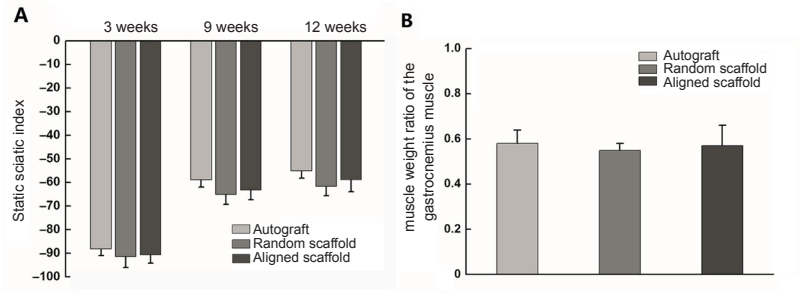

Figure 8 Static sciatic index and muscle weight ratio in rats with a sciatic nerve defect repaired with aligned or random nanofiber nerve guide conduits.
(A) Calculation of the static sciatic index. Static sciatic index value in healthy rats was 0. More negative static sciatic index values indicate worse neural function. (B) Calculation of the muscle weight ratio of the gastrocnemius muscle at 12 weeks. Data are expressed as the mean ± SEM (one-way analysis of variance).

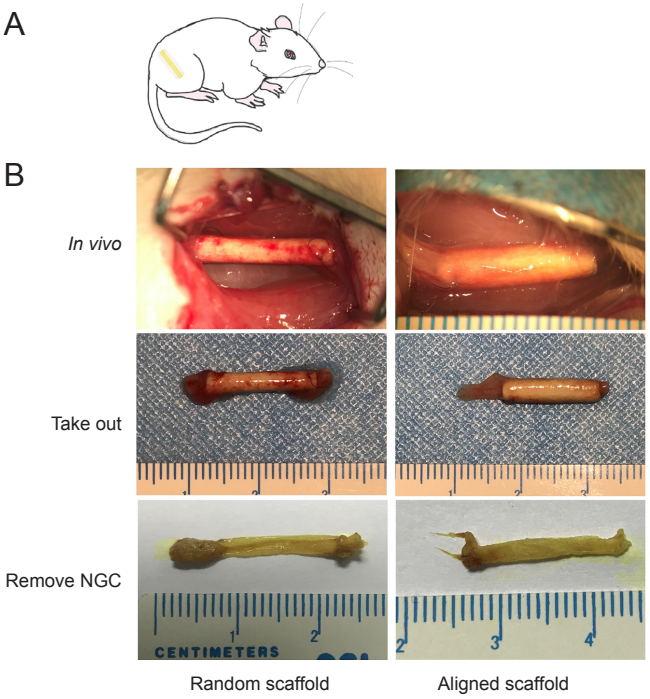

Figure 9 View of the regenerating sciatic nerve in rats implanted with aligned or random nanofiber NGCs.
(A) Illustration of NGC transplantation. (B) Gross observation of NGC-mediated repair of the sciatic nerve 120 days after surgery. NGC: Nerve guide conduit.

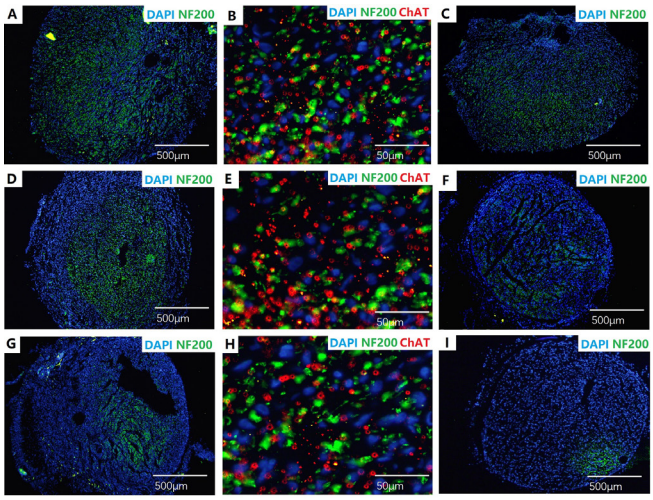

Figure 10 Labeling of histological cross-sections for NF200 (green, Alexa Fluor-488), ChAT (red, Alexa Fluor-594) and DAPI (blue) in rats implanted with aligned or random nanofiber nerve guide conduits.
Sections taken from the autograft group (A–C), aligned scaffold group (D–F), and random scaffold group (G–I). A, D and G: mid-guide region; C, F and I: approximately 1 mm proximal to the distal suture; B, E and H: approximately 1 mm proximal to the distal suture, with NF200 (green), ChAT (red) and DAPI (blue) merged. Scale bars: 500 μm in A, C, D, F, G, I; 50 μm in B, E, H. NF200: Neurofilament 200; ChAT: choline acetyltransferase; DAPI: 4′,6-diamino-2-phenylindole.

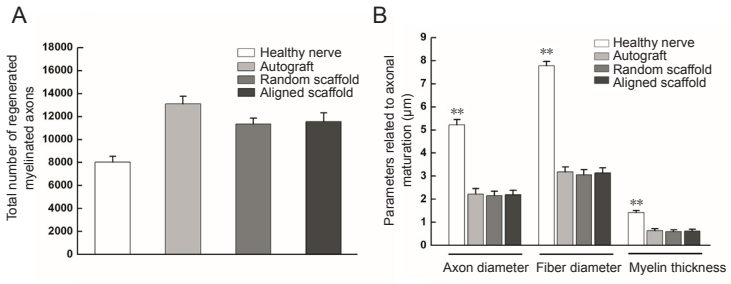

Figure 11 Morphometric analyses of the distal sciatic nerve, 5 mm from the nerve guide conduit, in rats implanted with aligned or random nanofiber nerve guide conduits.
(A) Total number of regenerated myelinated axons. (B) Parameters related to axonal maturation. Data are expressed as the mean ± SEM (one-way analysis of variance). $^{**}P < 0.01$, *vs.* healthy nerve.

Discussion

The history of the use of nerve guide conduits to repair nerve defects spans more than 100 years (Daly et al., 2012). Over the past 40 years, a variety of new materials, designs and techniques have been used to produce nerve guide conduits (Cai et al., 2005; Haastert-Talini et al., 2013). Recent studies have focused on optimizing nerve guide conduits to achieve therapeutic effects comparable to those of autografts. This goal has not yet been fully achieved (Haastert-Talini et al., 2013; Gu et al., 2014; Chen and Shen, 2017). However, conduits do appear to be effective for short nerve gaps (Bontioti et al., 2003; Battiston et al., 2007; Tos et al., 2007).

It is encouraging that the field of nerve guide conduit repair continues to consistently produce a wide variety of innovative techniques and novel conduit designs for the reconstruction of peripheral nerve defects. Intraluminal guidance structure is a promising option for building ideal nerve scaffolds (de Ruiter et al., 2008; Jeffries and Wang, 2012; Haastert-Talini et al., 2013). For example, chitosan films within chitosan nerve guides have been successful in bridging rat sciatic nerve defects of approximately 15 mm (Meyer et al., 2016). Silk as the guide fiber to establish a native-like microenvironment for nerve regeneration has also been demonstrated (Madduri et al., 2010; Wang et al., 2013). In the present study, we hypothesized that positioning aligned nanofibers within the nerve scaffold would yield a structure that enhances the intraluminal guidance of axons for the repair of peripheral nerve defects. The electrospun fibers help improve the interaction between the host tissue and the guide conduit (Georgiou et al., 2015). Electrospun technology is versatile and superior for the production and construction of complex nanofiber modules compared with other nanofiber fabrication processes (Jeffries and Wang, 2012; Georgiou et al., 2015; Quan et al., 2016). Nerve guide conduits constructed by tissue engineering and fabricated by electrospinning are highly porous and have a high surface area-to-volume ratio (Yang et al., 2005; Quan et al., 2016). Importantly, nerve guide conduits have an ability similar to extracellular matrix in allowing for the diffusion of nutrients and the removal of cellular metabolic waste (Chen et al., 2016). Furthermore, nerve guide conduits can limit the migration of fibroblasts. Another potential benefit is that electrospun fibers stimulate the formation of fiber cables during nerve regeneration, which could guide Schwann cell migration and alignment (Kim et al., 2008; Cao et al., 2010). This may account for why aligned nanofiber nerve guide conduits allow for the formation of continuous regenerative tissue earlier than random nanofiber nerve guide conduits.

Polycaprolactone is a biodegradable polyester with good biocompatibility. Under physiological conditions, polycaprolactone is degraded, and consequently, its use as an implantable biomaterial has received great attention. Polycaprolactone electrospun fiber has high tensile strength, is nontoxic, and has good biodegradability. Moreover, polycaprolactone has been approved by the Food and Drug Administration for use in the human body.

There are a variety of bioengineered nerve guide conduits with Food and Drug Administration approval for clinical use. Recent clinical feedback from surgeons suggest that the failure of nerve guide conduits could be attributed to luminal volume decrease, suture pull-out with traction during movement, conduit collapse, and swelling produced by the biomaterial (Shim et al., 2015; Clements et al., 2016). In the present study, we used electrospinning to produce the nerve guide conduits. Because of the advantageous characteristics of electrospun fibers and polycaprolactone, including high tensile strength, non-toxicity and biodegradability, these new nerve guide conduits might overcome some of the current clinical limitations.

Most rat models of nerve defects involve the sciatic, median and facial nerves. Upper limb nerve defect models are amenable to objective functional studies (Papalia et al., 2003; Geuna et al., 2007; Papalia et al., 2016). Our objective in this study was to repair a 15-mm nerve defect, which is longer than the median nerve. To repair a 15-mm defect in the median nerve, we must cross the joint. This will increase the mechanical requirements of the nerve guide conduit to ensure that the joint movement does not affect its structural integrity.

In vitro mechanical tests showed that the nerve guide conduit was suitable for suturing and for supporting sciatic nerve growth in rats. Nerve guide conduits have a high mechanical strength that reduces the risk of collapse. We believe that this ability may be attributable to the highly aligned fibers. The mechanical strength helps maintain the space within the conduit necessary for peripheral nerve regeneration. It also helps maintain the spatial organization of the aligned fibers. In the tensile strength tests, a turning point was detected in the aligned scaffold group, caused by breakage of the oriented fibers during stretching. In compression tests, performance was also better in the aligned scaffold group than in the random scaffold group. The 100-cycle compression test did not show a decrease in performance.

In *in vitro* experiments, Schwann cells, PC12 cells and dorsal root ganglions were seeded on aligned and random scaffolds for 1 week. Immunofluorescence staining revealed that the Schwann cells were oriented along the aligned fibers. As Schwann cells guide regenerating axons, this topology should promote the oriented growth of the regenerating axons and nerve bundle. Furthermore, the aligned scaffolds could guide the growth of new axons in PC12 cells and dorsal root ganglions. This ability could explain why, in the distal nerve segment, neurofilament-positive fibers were detected in 100% (7/7) of the aligned nanofiber nerve guide conduits at 49 days.

At 49 days, the proportion of regenerating axons extending to the distal nerve tissue was significantly higher in the aligned scaffold group than in the random scaffold group. In addition, the higher proportion of activated Schwann cells, which attract regenerating axons, likely also promoted nerve repair in the aligned groups (Saito and Dahlin, 2008; Tsuda et al., 2011). Furthermore, the proportion of apoptotic Schwann cells was lower in the aligned scaffold group than in the random scaffold group. Over 28 days, we found that almost all of the aligned scaffolds contained continuous regenerative

tissue, while the random scaffolds did not in the middle zone.

The presence of foot ulcers was higher in the random scaffold group than in the aligned scaffold group, which may be associated with comparatively lower nerve regeneration. In the natural repair process, a fibrin-based cable connects the two nerve stumps to accelerate the migration and proliferation of Schwann cells to form the bands of Büngner prior to axonal regeneration (Schnell et al., 2007; Coleman and Freeman, 2010; Shapira et al., 2016). The aligned fibers likely supported Schwann cell migration across the nerve defect and the formation of the regenerative fibrin matrix within the conduit.

The aligned nanofiber nerve guide conduits showed better results in short-term functional experiments compared with the random nanofiber nerve guide conduits. The static sciatic index and gastrocnemius muscle weight analyses showed that functional recovery was similar in rats transplanted with aligned nanofiber nerve guide conduits and autografts; however, the differences among the groups were not statistically significant. Immunofluorescence analysis showed motor nerve recovery in all groups. The total number of regenerating myelinated axons, axon diameter, fiber diameter and myelin thickness were significantly different between the healthy and implanted (autograft, aligned scaffold, and random scaffold) groups. The electrospun nerve guide conduits produced similar results as autografts, which are currently the gold standard. The permeability of electrospun nerve guide conduits might contribute to their effectiveness.

Previous studies suggest that added filler is effective; thus, it will be useful to explore aligned fiber fillers in future studies to accelerate nerve repair. Furthermore, future studies are needed to evaluate the impact of the various electrospinning parameters on nerve repair.

Regeneration involves neuronal growth and the formation of the extracellular matrix scaffold (Gu et al., 2014). The new nerve is formed by the migration of SCs, the formation of new blood vessels, and axonal outgrowth into a matrix of fibrin, which are basic requirements for regeneration (Schnell et al., 2007). The purpose of nerve guide conduits is to simulate the regenerative microenvironment of the nerve to facilitate Schwann cell proliferation and differentiation, with a suitable porosity that limits scar formation. A recent study indicated that reconstruction of a severed nerve trunk may improve clinical outcomes (Johansson and Dahlin, 2014). In the present study, we developed a multi-step electrospinning process to fabricate nerve guide conduits. A cross-section of the luminal surface shows longitudinally aligned fibers for axon and Schwann cell guidance. This structure likely provides a better inner surface and greater mechanical stability than previous nerve conduits. These features enhance the regeneration of Schwann cells and axons. Therefore, our method might have potential application in neural tissue engineering.

Author contributions: *Study concept: QQ, HYM, QZ, and SBL; Data curation: QQ, BC, and GBL; formal analysis: QQ and HYM; funding acquisition: QZ, SBL, JP, and YW. Investigation: QQ, HYM, BC, and XQC. Methodology: QQ, HYM, and JP. Resources: QZ, SBL, JP, and YW. Software: QQ, BC, and HT. Supervision: QQ, SBL, and QZ. Validation: QQ and SBL. Visualization: QQ, HYM, HT, BC, and XQC. Writing and original draft: QQ, HYM, and YW. Writing, review and editing: QQ and HYM. All authors approved the final version of the paper.*
Conflicts of interest: *The authors declare that they have no conflict of interest.*
Financial support: *This study was supported by the National Natural Science Foundation of China, No. 31771052 (to YW); the National Basic Research Program of China (973 Program), No. 2014CB542201 (to JP); the National Key Research and Development Program of China, No. 2016YFC1101601 (to QZ), 2017YFA0104702 (to YW); the PLA General Hospital Translational Medicine Project of China, No. 2016TM-030 (to QZ); the Beijing Municipal Natural Science Foundation of China, No. 7172202 (to YW); the PLA Youth Training Project for Medical Science, China, No. 16QNP144 (to YW); the Beijing Municipal Science and Technology Project, China, No. Z161100005016059 (to YW). The funders had no role in the study design, data collection or analysis; the decision to publish; or the preparation of the manuscript.*
Institutional review board statement: *This study was approved by the Ethics Committee of the Chinese PLA General Hospital, Beijing, China (approval number: 2016-x9-07) in September, 2016.*
Copyright license agreement: *The Copyright License Agreement has been signed by all authors before publication.*
Data sharing statement: *Datasets analyzed during the current study are available from the corresponding author on reasonable request.*
Plagiarism check: *Checked twice by iThenticate.*
Peer review: *Externally peer reviewed.*

Open peer reviewer: *Michele R. Colonna, Universita degli Studi di Messina, Italy.*
Additional file: *Open peer review report 1.*

References

Ayres CE, Jha BS, Meredith H, Bowman JR, Bowlin GL, Henderson SC, Simpson DG (2008) Measuring fiber alignment in electrospun scaffolds: a user's guide to the 2D fast Fourier transform approach. J Biomater Sci Polym Ed 19:603-621.

Battiston B, Tos P, Conforti LG, Geuna S (2007) Alternative techniques for peripheral nerve repair: conduits and end-to-side neurorrhaphy. Acta Neurochir Suppl 100:43-50.

Bellamkonda RV (2006) Peripheral nerve regeneration: an opinion on channels, scaffolds and anisotropy. Biomaterials 27:3515-3518.

Bertleff MJ, Meek MF, Nicolai JP (2005) A prospective clinical evaluation of biodegradable neurolac nerve guides for sensory nerve repair in the hand. J Hand Surg Am 30:513-518.

Bontioti EN, Kanje M, Dahlin LB (2003) Regeneration and functional recovery in the upper extremity of rats after various types of nerve injuries. J Peripher Nerv Syst 8:159-168.

Cai J, Peng X, Nelson KD, Eberhart R, Smith GM (2005) Permeable guidance channels containing microfilament scaffolds enhance axon growth and maturation. J Biomed Mater Res A 75:374-386.

Cao H, McHugh K, Chew SY, Anderson JM (2010) The topographical effect of electrospun nanofibrous scaffolds on the in vivo and in vitro foreign body reaction. J Biomed Mater Res A 93:1151-1159.

Chang B, Quan Q, Lu S, Wang Y, Peng J (2016) Molecular mechanisms in the initiation phase of Wallerian degeneration. Eur J Neurosci 44:2040-2048.

Chen J, Shen H (2017) Tissue-engineered nerve conduits with internal structure in the repair of peripheral nerve defects. Zhongguo Zuzhi Gongcheng Yanjiu 21:1273-1279.

Chen W, Chen S, Morsi Y, El-Hamshary H, El-Newhy M, Fan C, Mo X (2016) Superabsorbent 3D scaffold based on electrospun nanofibers for cartilage tissue engineering. ACS Appl Mater Interfaces 8:24415-24425.

Chew SY, Mi R, Hoke A, Leong KW (2007) Aligned protein-polymer composite fibers enhance nerve regeneration: a potential tissue-engineering platform. Adv Funct Mater 17:1288-1296.

Chew SY, Mi R, Hoke A, Leong KW (2008) The effect of the alignment of electrospun fibrous scaffolds on Schwann cell maturation. Biomaterials 29:653-661.

Clements BA, Bushman J, Murthy NS, Ezra M, Pastore CM, Kohn J (2016) Design of barrier coatings on kink-resistant peripheral nerve conduits. J Tissue Eng 7:2041731416629471.

Coleman MP, Freeman MR (2010) Wallerian degeneration, wld(s), and nmnat. Annu Rev Neurosci 33:245-267.

Daly W, Yao L, Zeugolis D, Windebank A, Pandit A (2012) A biomaterials approach to peripheral nerve regeneration: bridging the peripheral nerve gap and enhancing functional recovery. J R Soc Interface 9:202-221.

de Luca AC, Terenghi G, Downes S (2014) Chemical surface modification of poly-epsilon-caprolactone improves Schwann cell proliferation for peripheral nerve repair. J Tissue Eng Regen Med 8:153-163.

de Ruiter GC, Spinner RJ, Malessy MJ, Moore MJ, Sorenson EJ, Currier BL, Yaszemski MJ, Windebank AJ (2008) Accuracy of motor axon regeneration across autograft, single-lumen, and multichannel poly(-lactic-co-glycolic acid) nerve tubes. Neurosurgery 63:144-155.

Deumens R, Bozkurt A, Meek MF, Marcus MA, Joosten EA, Weis J, Brook GA (2010) Repairing injured peripheral nerves: Bridging the gap. Prog Neurobiol 92:245-276.

Forciniti L, Ybarra J, 3rd, Zaman MH, Schmidt CE (2014) Schwann cell response on polypyrrole substrates upon electrical stimulation. Acta Biomater 10:2423-2433.

Georgiou M, Golding JP, Loughlin AJ, Kingham PJ, Phillips JB (2015) Engineered neural tissue with aligned, differentiated adipose-derived stem cells promotes peripheral nerve regeneration across a critical sized defect in rat sciatic nerve. Biomaterials 37:242-251.

Geuna S, Papalia I, Ronchi G, d'Alcontres FS, Natsis K, Papadopulos NA, Colonna MR (2017) The reasons for end-to-side coaptation: how does lateral axon sprouting work? Neural Regen Res 12:529-533.

Geuna S, Tos P, Raimondo S, Lee JM, Gambarotta G, Nicolino S, Fornaro M, Papalia I, Perroteau I, Battiston B (2007) Functional, morphological and biomolecular assessment of posttraumatic neuro-muscular recovery in the rat forelimb model. Acta Neurochir Suppl 100:173-177.

Gu X, Ding F, Williams DF (2014) Neural tissue engineering options for peripheral nerve regeneration. Biomaterials 35:6143-6156.

Haastert-Talini K, Geuna S, Dahlin LB, Meyer C, Stenberg L, Freier T, Heimann C, Barwig C, Pinto LF, Raimondo S, Gambarotta G, Samy SR, Sousa N, Salgado AJ, Ratzka A, Wrobel S, Grothe C (2013) Chitosan tubes of varying degrees of acetylation for bridging peripheral nerve defects. Biomaterials 34:9886-9904.

Jeffries EM, Wang Y (2012) Biomimetic micropatterned multi-channel nerve guides by templated electrospinning. Biotechnol Bioeng 109:1571-1582.

Johansson F, Dahlin LB (2014) The multiple silicone tube device, "tubes within a tube," for multiplication in nerve reconstruction. Biomed Res Int 2014:689127.

Kim YT, Haftel VK, Kumar S, Bellamkonda RV (2008) The role of aligned polymer fiber-based constructs in the bridging of long peripheral nerve gaps. Biomaterials 29:3117-3127.

Madduri S, Papaloizos M, Gander B (2010) Trophically and topographically functionalized silk fibroin nerve conduits for guided peripheral nerve regeneration. Biomaterials 31:2323-2334.

Meyer C, Stenberg L, Gonzalez-Perez F, Wrobel S, Ronchi G, Udina E, Suganuma S, Geuna S, Navarro X, Dahlin LB, Grothe C, Haastert-Talini K (2016) Chitosan-film enhanced chitosan nerve guides for long-distance regeneration of peripheral nerves. Biomaterials 76:33-51.

Papalia I, Tos P, Stagno d'Alcontres F, Battiston B, Geuna S (2003) On the use of the grasping test in the rat median nerve model: a re-appraisal of its efficacy for quantitative assessment of motor function recovery. J Neurosci Methods 127:43-47.

Papalia I, Magaudda L, Righi M, Ronchi G, Viano N, Geuna S, Colonna MR (2016) Epineurial window is more efficient in attracting axons than simple coaptation in a sutureless (cyanoacrylate-bound) model of end-to-side nerve repair in the rat upper limb: functional and morphometric evidences and review of the literature. PLoS One 11:e0148443.

Quan Q, Chang B, Meng HY, Liu RX, Wang Y, Lu SB, Peng J, Zhao Q (2016) Use of electrospinning to construct biomaterials for peripheral nerve regeneration. Rev Neurosci 27:761-768.

Ray WZ, Mackinnon SE (2010) Management of nerve gaps: autografts, allografts, nerve transfers, and end-to-side neurorrhaphy. Exp Neurol 223:77-85.

Saito H, Dahlin LB (2008) Expression of ATF3 and axonal outgrowth are impaired after delayed nerve repair. BMC Neurosci 9:88.

Schnell E, Klinkhammer K, Balzer S, Brook G, Klee D, Dalton P, Mey J (2007) Guidance of glial cell migration and axonal growth on electrospun nanofibers of poly-epsilon-caprolactone and a collagen/poly-epsilon-caprolactone blend. Biomaterials 28:3012-3025.

Shapira Y, Tolmasov M, Nissan M, Reider E, Koren A, Biron T, Bitan Y, Livnat M, Ronchi G, Geuna S, Rochkind S (2016) Comparison of results between chitosan hollow tube and autologous nerve graft in reconstruction of peripheral nerve defect: An experimental study. Microsurgery 36:664-671.

Shim SW, Kwon DY, Lee BN, Kwon JS, Park JH, Lee JH, Kim JH, Lee IW, Shin JW, Lee HB, Kim WD, Kim MS (2015) Evaluation of small intestine submucosa and poly(caprolactone-co-lactide) conduits for peripheral nerve regeneration. Tissue Eng Part A 21:1142-1151.

Stenberg L, Kodama A, Lindwall-Blom C, Dahlin LB (2016) Nerve regeneration in chitosan conduits and in autologous nerve grafts in healthy and in type 2 diabetic Goto-Kakizaki rats. Eur J Neurosci 43:463-473.

Tos P, Battiston B, Nicolino S, Raimondo S, Fornaro M, Lee JM, Chirila L, Geuna S, Perroteau I (2007) Comparison of fresh and predegenerated muscle-vein-combined guides for the repair of rat median nerve. Microsurgery 27:48-55.

Tsuda Y, Kanje M, Dahlin LB (2011) Axonal outgrowth is associated with increased ERK 1/2 activation but decreased caspase 3 linked cell death in Schwann cells after immediate nerve repair in rats. BMC Neurosci 12:12.

Wang K, Xu M, Zhu M, Su H, Wang H, Kong D, Wang L (2013) Creation of macropores in electrospun silk fibroin scaffolds using sacrificial PEO-microparticles to enhance cellular infiltration. J Biomed Mater Res A 101:3474-3481.

Wang W, Gao J, Na L, Jiang H, Xue J, Yang Z, Wang P (2014) Craniocerebral injury promotes the repair of peripheral nerve injury. Neural Regen Res 9:1703-1708.

Yang F, Murugan R, Wang S, Ramakrishna S (2005) Electrospinning of nano/micro scale poly(L-lactic acid) aligned fibers and their potential in neural tissue engineering. Biomaterials 26:2603-2610.

Zhu Y, Wang A, Patel S, Kurpinski K, Diao E, Bao X, Kwong G, Young WL, Li S (2011) Engineering bi-layer nanofibrous conduits for peripheral nerve regeneration. Tissue Eng Part C Methods 17:705-715.

P-Reviewer: Colonna MR; C-Editor: Zhao M; S-Editors: Yu J, Li CH; L-Editors: Patel B, Stow A, Qiu Y, Song LP; T-Editor: Liu XL